CERN - EUROPEAN ORGANIZATION FOR NUCLEAR RESEARCH

Submitted to
Nucl. Physics B.

CERN/EP/PHYS 77-46
5 September 1977

# A STUDY OF $\bar{n}p$ ANNIHILATIONS AROUND 0.65 GeV/c

Bombay-CERN-Neuchâtel-Tokyo Collaboration

R. HAMATSU, S. KITAMURA and T. YAMAGATA
Tokyo Metropolitan University, Setagayaku, Tokyo

M. BOGDANSKI and E. JEANNET
Institut de Physique de l'Université de Neuchâtel, Neuchâtel.

A.M. COOPER, S.N. GANGULI, A. GURTU, P.K. MALHOTRA, U. MEHTANI, R. RAGHAVAN and A. SUBRAMANIAN
Tata Institute of Fundamental Research, Bombay.

T. EMURA, I. KITA and K. TAKAHASHI
Tokyo University of Agriculture and Technology, Koganei, Tokyo.

H. KOHNO
Chuo University, Bunkyoku, Tokyo.

L. MONTANET
CERN, European Organization for Nuclear Research, Geneva.

## ABSTRACT

$\bar{n}p$ annihilations with $\geq 3$ prongs with an incident antineutron momentum between 0.5 and 0.8 GeV/c are analysed. We present the topological branching ratios and cross sections, the resonance production rates and possible $\rho$-$\omega$ interference effects.

LM/fv

## 1. INTRODUCTION

The data on $\bar{n}p$ annihilations are scanty [1,2]. Most of our knowledge comes in fact from the charge-symmetrical $\bar{p}n$ annihilations [3-20]. In this paper, we present some results obtained from $\bar{n}p$ annihilations, the antineutrons being produced in the charge exchange reaction $\bar{p}p \to \bar{n}n$ with incident antiprotons of 700 to 750 MeV/c. The data come from a series of exposures in the 81 cm Saclay hydrogen bubble chamber to a CERN antiproton beam. The $\bar{n}p$ annihilations take place free from deuteron complications so that in this case, it is possible to study antinucleon-nucleon annihilations of a pure isospin state (I=1) with a better energy and momentum resolution than in the $\bar{p}n$ case.

In this experiment we limit ourselves to 3, 5 and 7-prong annihilations corresponding to the following reactions:

$$\text{with} \quad \bar{n}p \to (n_1 + 1)\,\pi^+ + n_1\pi^- + n_2\pi^0 \qquad (1)$$

$$n_1 = 1,2,3 \text{ and } n_2 = 0,1, \text{ etc.}$$

The signature of these reactions in the bubble chamber is the occurrence of a vertex with an odd number of charged prongs due to a $\bar{n}p$ annihilation associated with an upstream zero-prong vertex ($\bar{p}p \to \bar{n}n$ charge exchange reaction). About 3500 such events were observed in 640 000 pictures. The total and differential cross sections for the charge exchange scattering are given in a previous paper [21], and experimental details are described elsewhere [22].

Fig. 1 shows the momentum distribution of the antineutrons produced in the $\bar{p}p$ charge exchange reactions. For the following analysis, we accepted the events with an incident antineutron momentum between 0.5 and 0.8 GeV/c.

## 2. TOPOLOGICAL BRANCHING RATIOS AND CROSS SECTIONS

Topological branching ratios for the $\bar{n}p$ annihilation, i.e., ratios of 5-prong and 7-prong to 3-prong events are given in table 1. They are in good agreement with the ratios obtained in the $\bar{p}n$ experiment between 0.4 and 0.9 GeV/c [14] and with the predictions of the Orfanidis-Rittenberg statistical model [23].

Topological cross sections were deduced as follows. The number and the track length of the incident antineutrons are not known, since they are recognized only when they give rise to a star within the fiducial volume. In our previous publication [21] we have used the annihilation cross section for $\bar{n}p$ giving rise to $\geq 3$ prongs as $\frac{747}{\sqrt{T}}$ in mb, where T is the kinetic energy of $\bar{n}$ in MeV, in order to deduce the charge exchange ($\bar{p}p \to \bar{n}n$) cross section. The above form was deduced by Bizzarri et al. [11] from $\bar{p}n$ annihilation studies and is also in good agreement with the experimental results of Caro et al. [14]. By folding the $\bar{n}$ momentum distribution (see fig. 1) to the above form we calculated the topological cross sections and they are listed in table 1.

Topological cross sections for $\bar{p}p$ annihilations can also be measured in our experiment, except for zero-prong annihilations for which we use the results of Alston-Garnjost et al. [24]. For the two-prong annihilations, we have subtracted the elastic scattering cross section [22]. Our results are in fair agreement with the Orfanidis-Rittenberg model (see table 2).

## 3. EXCLUSIVE FINAL STATES

### 3.1 $\bar{n}p \to 2\pi^+\pi^-$

A sample of 85 events corresponding to the reaction

$$\bar{n}p \to \pi^+\pi^+\pi^- \qquad (2)$$

was obtained. Fig. 2 shows the Dalitz plot for this reaction and the corresponding effective mass spectra.

The Dalitz plot shows a depletion of events at $s \sim t \sim 1$ GeV$^2$ and a concentration of events in the $\rho$ and f mass bands. These features are similar to those observed in $\bar{p}n \to \pi^-\pi^-\pi^+$ at rest [4] as well as at 1.2 GeV/c [5]. All these features can be interpreted with the help of dual amplitudes à la Veneziano [22]. We find that our data are consistent with a $2^+$ amplitude of the form

$$A^{ij}(s,t) = \frac{\Gamma\left(2-\alpha_\rho(s)\right)\Gamma\left(1-\alpha_\rho(t)\right)}{\Gamma\left(3-\alpha_\rho(s)-\alpha_\rho(t)\right)}\left(p_2^i q^j + p_1^j q^i\right)$$

$$- \frac{\Gamma\left(1-\alpha_\rho(s)\right)\Gamma\left(2-\alpha_\rho(t)\right)}{\Gamma\left(3-\alpha_\rho(s)-\alpha_\rho(t)\right)}\left(p_2^i q^j + p_2^j q^i\right) \quad ,$$

where $\alpha_\rho(s) = 0.65 + 0.84\, s + i\, 0.26 \sqrt{s - 4\, m^2}$

$s = M^2(\pi_1^+\pi^-)$ ; $t = M^2(\pi_2^+\pi^-)$

$p_1, p_2$ = momenta of the $\pi^+$'s in CMS

$q = p_2 \times p_1$.

The curves shown in fig. 2 correspond to this amplitude and reproduce our data qualitatively.

### 3.2 $\bar{n}p \to 2\pi^+\pi^-\pi^0$

A sample of 502 events corresponding to the reaction

$$\bar{n}p \to 2\pi^+\pi^-\pi^0 \qquad (3)$$

was obtained. Fig. 3 shows the $(\pi^+\pi^-)$, $(\pi^+\pi^0)$, $(\pi^-\pi^0)$ and $(\pi^+\pi^-\pi^0)$ mass distributions. A sizeable production of $\rho^0$ and $\rho^+$ is observed.

Resonance production using maximum likelihood fit to this reaction is summarized in table 3. From this it is seen that the ρ production is the most dominant one and can account for ≈ 60% of the events, whereas the production of $f^0$ and $\omega^0$ together is ≈ 10%. In an attempt to interpret these results, we have used the multiperipheral model [25,26], pertaining to the diagrams shown in fig. 4. Since the multiperipheral model does not fix the relative phases of the contributing diagrams, we use the sum of the matrix element squared and introduce the relevant phase-space and Breit-Wigner factors. We use the parameters introduced by De la Vaissière and which should be relevant to our incident momentum range. The results of the fit are shown in fig. 3 and are in good agreement with our experimental data.

### 3.3 $\bar{n}p \to 3\pi^+2\pi^-$, $\bar{n}p \to 3\pi^+2\pi^-\pi^0$

A sample of 179 events corresponding to the reaction

$$\bar{n}p \to 3\pi^+2\pi^- \qquad (4)$$

was obtained. Fig. 5 shows the $(\pi^+\pi^-)$, $(2\pi^+\pi^-)$, $(\pi^+2\pi^-)$ and $(2\pi^+2\pi^-)$ mass distributions. We note that these distributions deviate significantly from pure phase-space without, however, showing any convincing resonance production. These effects have been observed in previous annihilation analyses and can be explained in terms of dual amplitudes [27]. These effects are more pronounced in the reactions where there are no neutral states in the initial and final states ($\bar{p}p$, $\pi^0$) as for reactions (2) and (4) and their charge conjugates. On the contrary, reactions with initial or final neutral states exhibit a more pronounced resonance production. This is the case for $\bar{p}p$ annihilations into any final state and also the case for reactions (3) and (5)

$$\bar{n}p \to 3\pi^+2\pi^-\pi^0 \ . \qquad (5)$$

In all 287 events corresponding to reaction (5) were observed. Fig. 6 shows the $(\pi^+\pi^-)$, $(\pi^+\pi^0)$, $(\pi^-\pi^0)$ and $(\pi^+\pi^-\pi^0)$ mass distributions. The $\omega^0 \to \pi^+\pi^-\pi^0$ accounts for 45% of this reaction.

## 4. ρ-ω INTERFERENCE EFFECTS

Opat has shown that the G-parity conservation in $\bar{p}n$ reactions implies a beam target symmetry or effectively a forward-backward symmetry for particles or groups of particles which are eigenstates of G [20]. One can therefore expect that to any ρ-ω constructive interference in the forward direction there should correspond a destructive interference in the backward direction and vice-versa. Integrated over all directions, the interference effects should vanish. Caro et al. [20] have applied these remarks to $\bar{p}d$ annihilations. Fig. 7 suggests that we observe these effects in $\bar{n}p \to 2\pi^+\pi^-\pi^0$. The forward $(\pi^+\pi^-)$ mass distribution differs from the backward one in the ω-mass region. We made a quantitative test by fitting the following function into the distributions of fig. 7 from threshold to 1.08 GeV where $f^0$ production distorts the shape of the background

$$\frac{dN}{dm} = \frac{dN}{dm}\,(\text{forward}) + \frac{dN}{dm}\,(\text{backward})$$

with
$$\frac{dN}{dm}\begin{pmatrix}\text{forward}\\ \text{backward}\end{pmatrix} = \left(A_\omega^2 BW_\omega^2 + A_\rho^2 BW_\rho^2 \pm 2A_\omega A_\rho \mathrm{Re}\left(e^{i\varphi} BW_\omega BW_\rho^*\right) + B\right) \text{P.S.}$$

$BW_\omega$ and $BW_\rho$ are the Breit-Wigner amplitudes for ω and ρ respectively and P.S. the phase-space with the beam profile folded in

$$BW_\omega = \frac{\Gamma_\omega^{\frac{1}{2}}}{\left(m_\omega^2 - m^2\right) - i m_\omega \Gamma_\omega}$$

$$BW_\rho = \frac{\Gamma_\rho^{\frac{1}{2}}}{\left(m_\rho^2 - m^2\right) - i m_\rho \Gamma_\rho} \quad ,$$

where $m_\omega$ = 784 MeV, $\Gamma_\omega$ = 10 MeV, $m_\rho$ = 770 MeV. For the width of ρ, we used

$$\Gamma_\rho = \Gamma_o \frac{m_\rho}{m}\left(\frac{q}{q_\rho}\right)^3 \quad \text{with } \Gamma_o = 146 \text{ MeV}.$$

The fit gives the following results:

$A_\omega = 0.17 \pm 07$ $\quad A_\rho = 1.11 \pm .09$

$\phi = 1.25 \pm 95$ $\quad B = 408 \pm 16$

$\chi^2/ND = 36/36$

and is represented by the curves in fig. 7. The numbers of $\rho$ and $\omega$ events were obtained by integrating over the fitted range of $\pi^+\pi^-$ effective mass. These are

$$N_\omega = 8 \pm 2; \qquad N_\rho = 142 \pm 6$$

It is to be remarked that if the distributions of fig. 7 are fitted without the $\rho$-$\omega$ intereference the value of $\chi^2/ND$ reaches 51/38 a poorer fit than the fit obtained with the $\rho$-$\omega$ interference.

## 5. DISCUSSION AND CONCLUSIONS

The results of our analysis of $\bar{n}p$ annihilations around 0.65 GeV/c lead to the following conclusions:

(a) The topological branching ratios for $\bar{n}p$ annihilations are in agreement with those for $\bar{p}n$ annihilations and the statistical model of Orfanidis and Rittenberg gives good predictions for these data.

(b) The $\bar{n}p$ annihilations with no $\pi^o$ in the final state ($\bar{n}p \to 2\pi^+\pi^-$, $3\pi^+2\pi^-$) are difficult to interpret in terms of classical resonance production. This is also the case for $\bar{p}n \to 2\pi^-\pi^+$ and it may indicate that dual amplitude effects are important for these final states.

(c) $\bar{n}p$ annihilations into $2\pi^+\pi^-\pi^o$ and $3\pi^+2\pi^-\pi^o$ show an abundant resonance production. The four pion annihilations are qualitatively well described by the multiperipheral model. (The six pion annihilations would require the introduction of too many diagrams to make this test significant).

(d) The $(\pi^+\pi^-)$ mass distribution for $\bar{n}p \to 2\pi^+\pi^-\pi^0$ shows possible $\rho$-$\omega$ interference effects.

We acknowledge the good work of our scanning and measuring teams. The Tokyo groups have been assisted by a grant of the Japan Society for the Promotion of Science and of the Mitsubishi Foundation.

REFERENCES

[1] S.P. Denison et al., Phys. Lett. 34B (1972) 167.

[2] A. Colebourn, Ph.D. Thesis (Liverpool) (1970).

[3] W. Chinowsky and G. Kojoan, Nuovo Cim. 43A (1966) 684.

[4] P. Anninos et al., Phys. Rev. Lett. 20 (1968) 402.

[5] A. Bettini et al., Nuovo Cim. 42A (1966) 695.

[6] A. Bettini et al., Nuovo Cim. 47A (1967) 692.

[7] A. Bettini et al., Nuovo Cim. 62A (1969) 1038.

[8] R. Bizzarri et al., Phys. Rev. Lett. 25 (1970) 1385.

[9] J. Roy and G. Tzanakos, Phys. Rev. Lett. 33 (1974) 1631.

[10] Th. Papadopoulou et al., Phys. Lett. 43B (1973) 401.

[11] R. Bizzarri et al., Nuovo Cim. 22A (1974) 225.

[12] R.D. Burrows et al., Austral. J. Phys. 23 (1970) 819.

[13] J.L. Atchison et al., Lett. Nuovo Cim. 2 (1971) 1009.

[14] D.E. Caro et al., Nucl. Phys. B90 (1975) 221.

[15] A. Bettini et al., Nucl. Phys. 1A (1975) 333.

[16] L. Bertaniza et al., Nuovo Cim. 23A (1974) 209.

[17] R.H. Huesman et al., Nuovo Cim. 25A (1975) 91.

[18] G. Borreani et al., Nuovo Cim. 10 (1974) 529.

[19] P.S. Eastman et al., Nucl. Phys. B51 (1973) 29.

[20] D.E. Caro et al., Proc. of the IVth Int. Symposium on $\bar{N}N$ Interactions, Syracuse 1975 (III-13).

[21] M. Bogdanski et al., Phys. Lett. B63 (1976) 117.

[22] S. Kitamura, D.Sc. Thesis, Tokyo Metropolitan University (1976) unpublished.

[23] S.J. Orfanidis and V. Rittenberg, Nucl. Phys. B59 (1973) 570.

[24] M. Alston-Garnjost et al., Phys. Rev. Lett. 35 (1975) 1685.

[25] Ch. de la Vaissière, Nouvo Cim. 11A (1972) 185.

[26] Ch. de la Vaissière, Nuovo Cim. 19A (1974) 118.

[27] see for instance H. Rubinstein - Symposium on Antinucleon-nucleon Interactions, Prague 1974, Yellow Report CERN 74-18, 232.

TABLE CAPTIONS

Table 1 Topological branching ratios and cross sections.

Table 2 Topological branching ratios for $\bar{p}p$ annihilations at 0.7 GeV.

Table 3 Channel fit to the reaction $\bar{n}p \to 2\pi^+\pi^-\pi^o$.

Table 1

| Topology | $\bar{n}p$ ratio | $\bar{n}p$ cross section (mb) | $\bar{p}n$ ratio [14] | OR model |
|---|---|---|---|---|
| 3 prongs | 1 | 36.8 ± 1.4 | 1 | 1 |
| 5 prongs | 0.42 ± 0.02 | 15.3 ± 0.9 | 0,36 ± 0,03 | 0,376 |
| 7 prongs | 0.014± 0.03 | 0.5 ± 0.2 | - | 0,016 |

Table 2

| Topology | cross section (mb) | ratio % | OR model (%) |
|---|---|---|---|
| 0 prong | 2.63 ± 0.07 [27] | 3,7 ± 0,1 | 2,7 |
| 2 prongs | 27,6 ± 1,7 | 38,6 ± 2,4 | 43.0 |
| 4 prongs | 37.6 ± 0,6 | 52,5 ± 0,8 | 47.6 |
| 6 prongs | 3.6 ± 0,2 | 5,0 ± 0,3 | 6,6 |
| 8 prongs | 0.04 ± 0.02 | 0,06± 0.03 | 0,09 |

Table 3

| Reaction channel | Fraction (%) |
|---|---|
| $\bar{n}p \rightarrow \rho^{o}\pi^{+}\pi^{-}$ | 11.6 ± 6.7 |
| $\rightarrow \rho^{+}\pi^{+}\pi^{-}$ | 15.8 ± 6.6 |
| $\rightarrow \rho^{-}\pi^{+}\pi^{+}$ | 9.6 ± 3.8 |
| $\rightarrow \rho^{+}\rho^{o}$ | 20.2 ± 5.7 |
| $\rightarrow f^{o}\pi^{+}\pi^{o}$ | 4.8 ± 2.7 |
| $\rightarrow \omega^{o}\pi^{+}$ | 4.4 ± 1.4 |
| $\rightarrow 2\pi^{+}\pi^{-}\pi^{o}$ | 33.6 ± 7.3 |

FIGURE CAPTIONS

Fig. 1 Momentum distribution of the antineutrons. The two arrows indicate the momentum criterion imposed for acceptance of events. The abnormal excess of events of $\bar{n}$ momentum < 0.02 GeV/c is due to erroneous fits in the kinematical fitting procedure [21,22].

Fig. 2 (a) Dalitz plot for the reaction $\bar{n}p \to 2\pi^+\pi^-$ at 0.65 GeV/c. The contours give the prediction by the $2^+$ amplitude.

(b) Projection of the folded Dalitz plot for the $(\pi^+\pi^-)$ effective mass squared.

(c) Projection of the Dalitz plot for the $(\pi^+\pi^+)$ effective mass squared. The solid and dashed curves in both (b) and (c) are the predictions for the $2^+$ amplitude and phase space respectively.

Fig. 3 (a) $(\pi^+\pi^-)$, (b) $(\pi^+\pi^0)$, (c) $(\pi^-\pi^0)$, (d) $(\pi^+\pi^-\pi^0)$ effective mass distributions for $\bar{n}p \to 2\pi^+\pi^-\pi^0$. The curves represent the fit obtained for a multiperipheral production [25,26].

Fig. 4 Graphs for the multiperipheral model contributing to the reaction $\bar{n}p \to 2\pi^+\pi^-\pi^0$.

Fig. 5 (a) $(\pi^+\pi^-)$, (b) $(\pi^+\pi^+\pi^-)$, (c) $(\pi^+\pi^-\pi^-)$, and (d) $(\pi^+\pi^+\pi^-\pi^-)$ effective mass distributions for $\bar{n}p \to 3\pi^+2\pi^-$. The curves represent the phase space.

Fig. 6 (a) $(\pi^+\pi^-)$, (b) $(\pi^-\pi^0)$, (c) $(\pi^+\pi^0)$, and (d) $(\pi^+\pi^-\pi^0)$ effective mass distributions for $\bar{n}p \to 3\pi^+2\pi^-\pi^0$. The curves represent the phase space.

Fig. 7 $(\pi^+\pi^-)$ effective mass spectra events with the $(\pi^+\pi^-)$ dipion system emitted: (a) in the forward direction and (b) in the backward direction for the $2\pi^+\pi^-\pi^0$ sample. The curves are obtained with the fit described in the text.

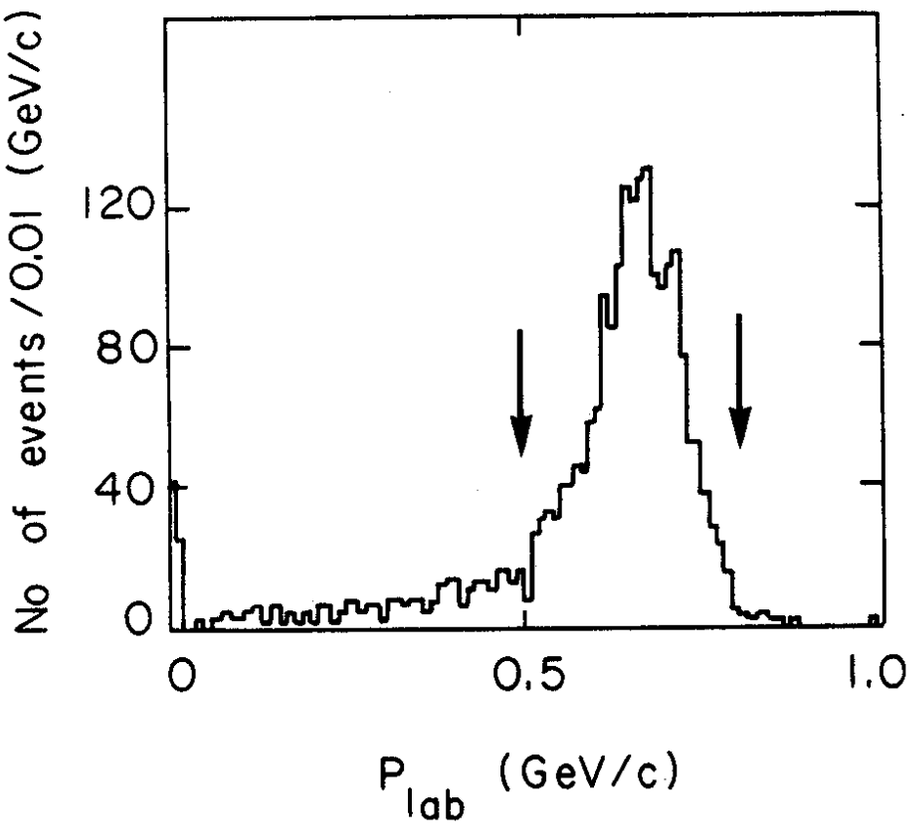


FIG.1

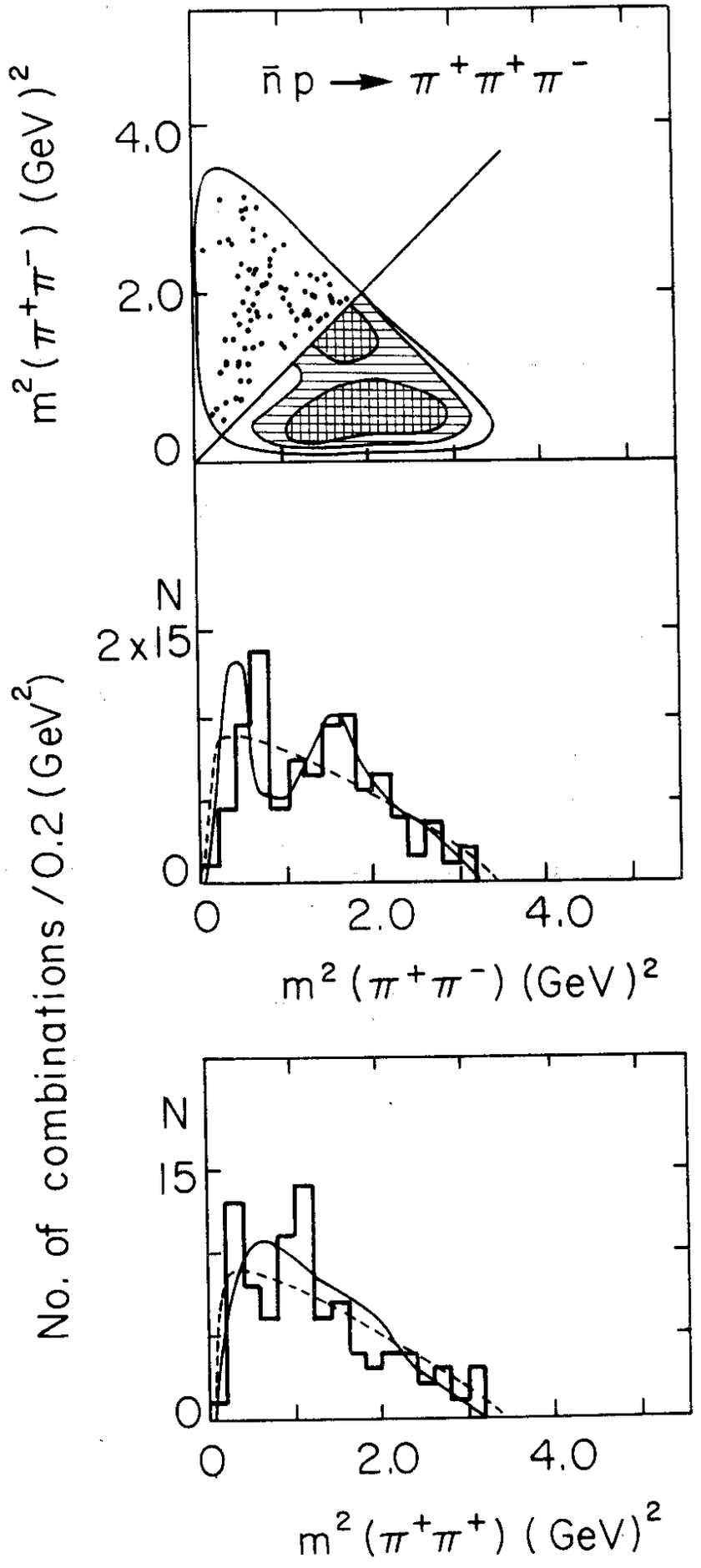
$\bar{n}p \rightarrow \pi^+\pi^+\pi^-$
$m^2(\pi^+\pi^-)$ (GeV)$^2$
4.0
2.0
0
N
2x15
0
2.0
4.0
$m^2(\pi^+\pi^-)$ (GeV)$^2$
No. of combinations /0.2 (GeV$^2$)
N
15
0
2.0
4.0
$m^2(\pi^+\pi^+)$ (GeV)$^2$

FIG. 2

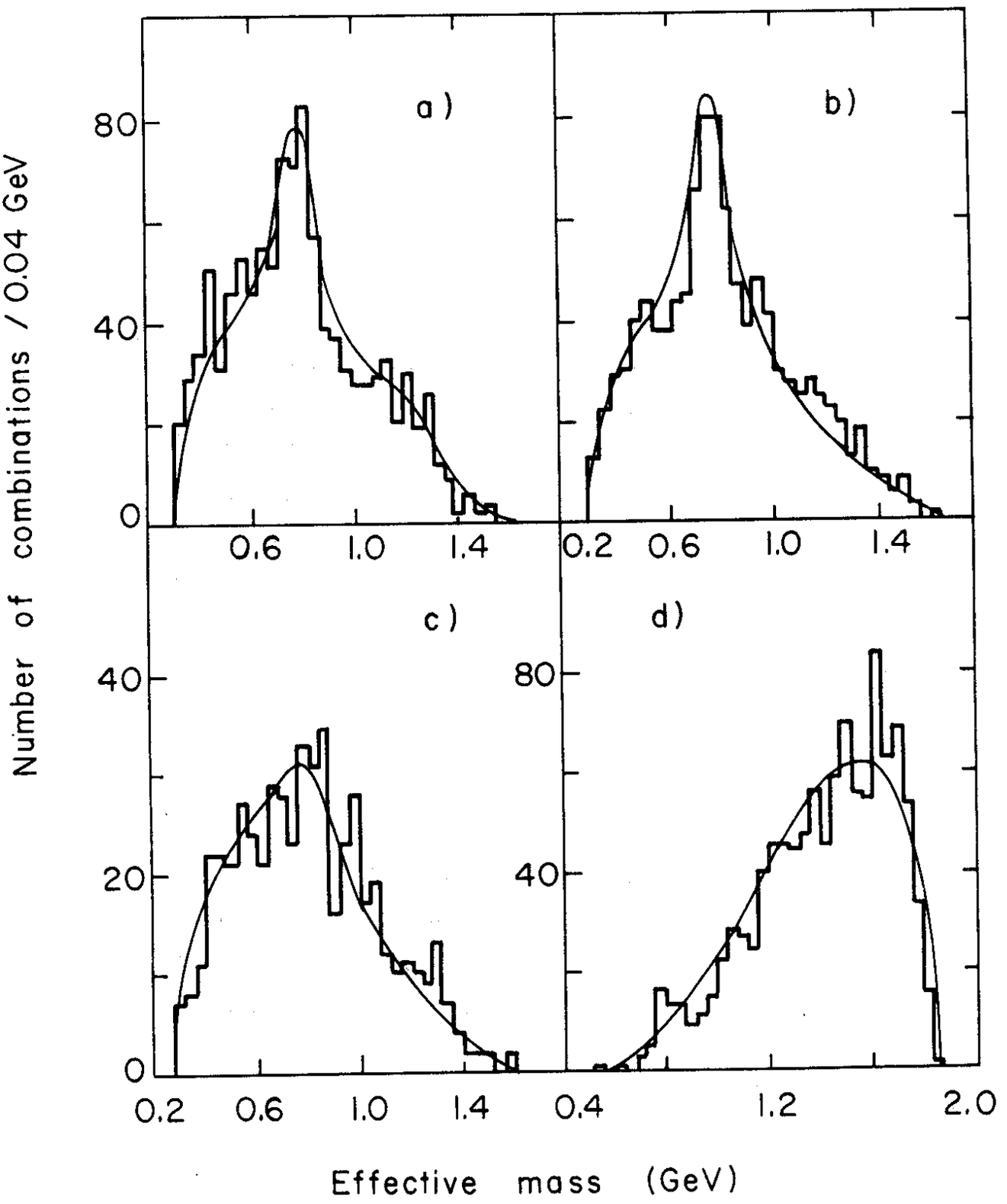
a)
b)
c)
d)
80
40
0
20
0.2
0.6
1.0
1.4
0.4
1.2
2.0
Number of combinations / 0.04 GeV
Effective mass (GeV)

FIG. 3

two body states


three body states

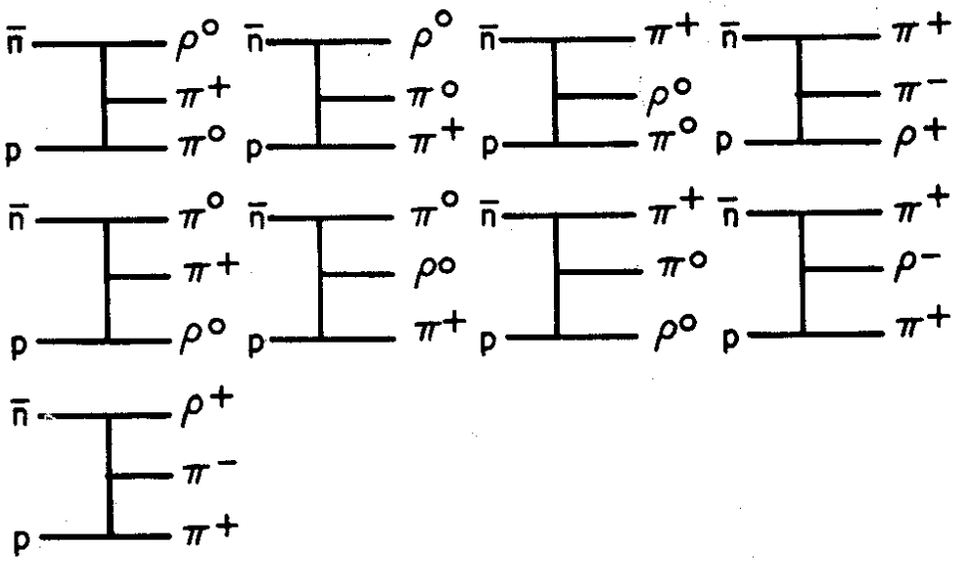


four body states

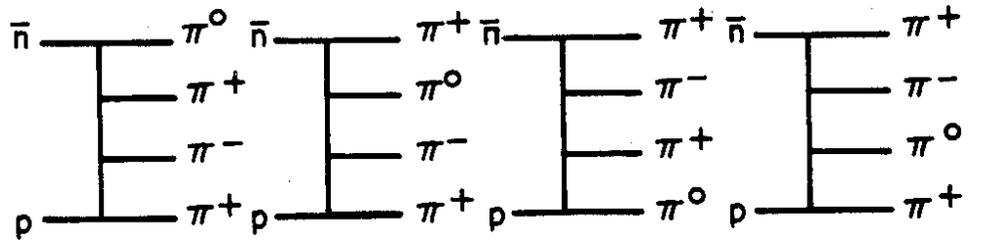


FIG. 4

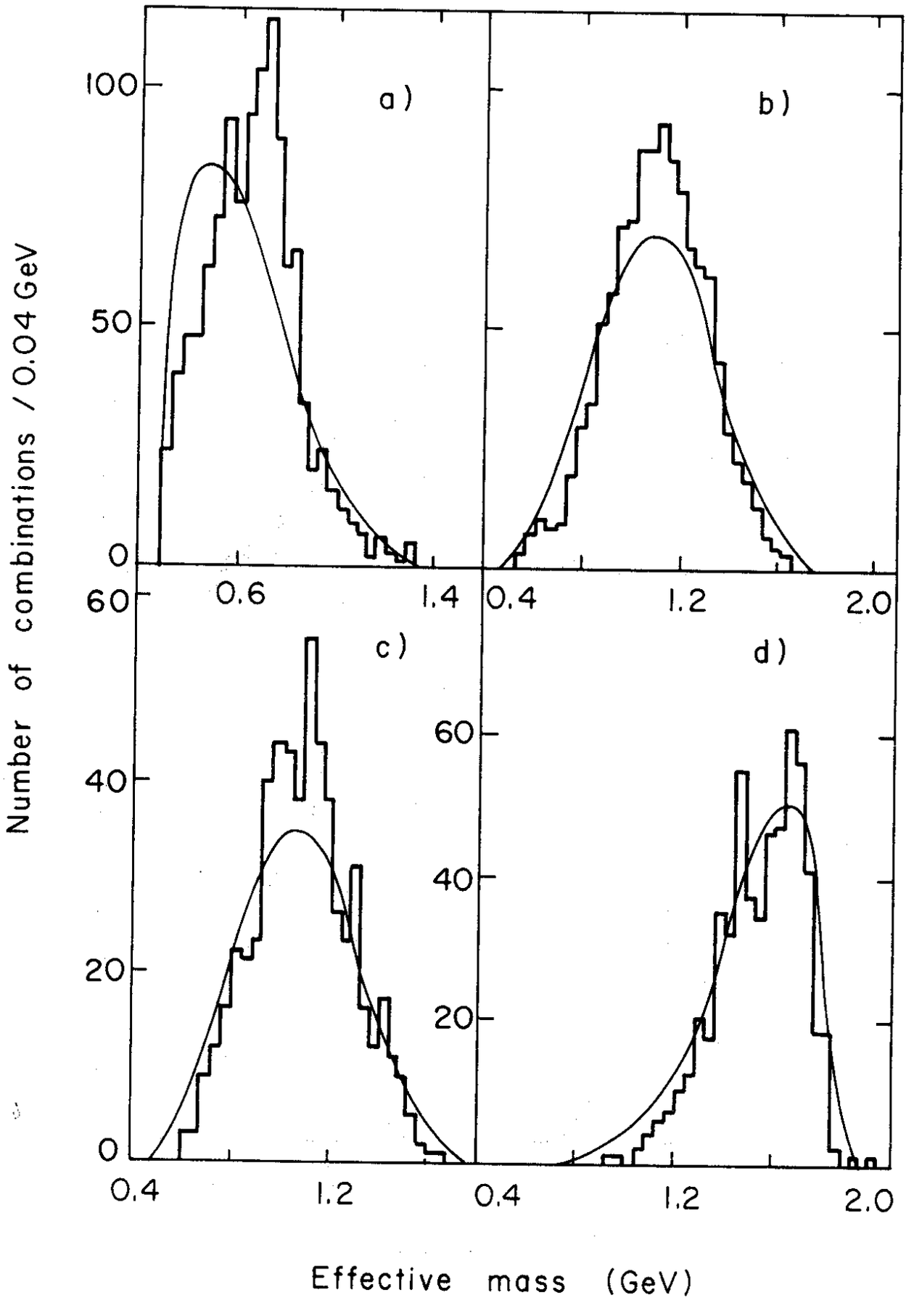
a)
b)
c)
d)
100
50
0
60
40
20
0
0.6
1.4
0.4
1.2
2.0
Number of combinations / 0.04 GeV
Effective mass (GeV)

FIG. 5

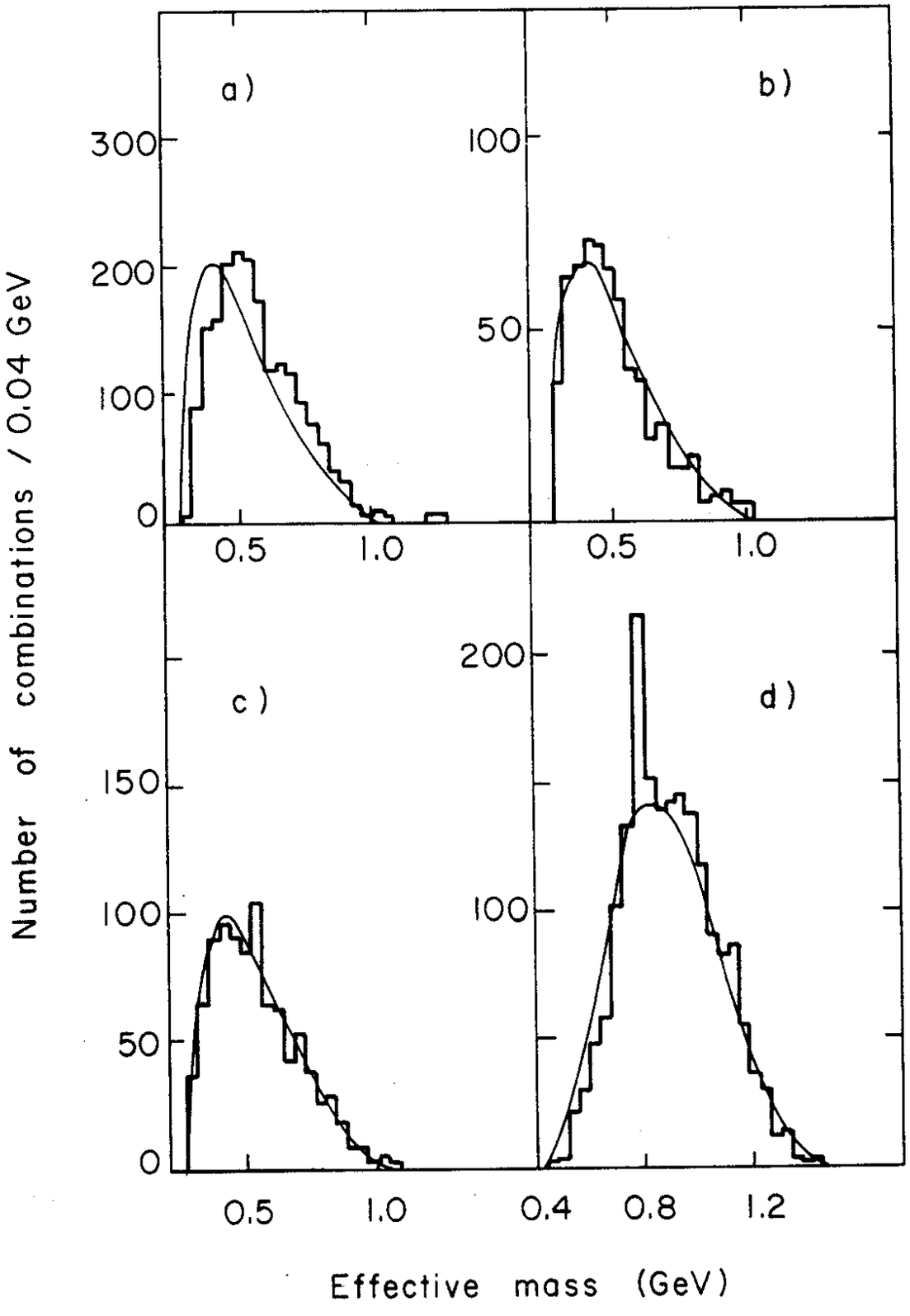
a)
b)
c)
d)
300
200
100
0
50
150
0.5
1.0
0.4
0.8
1.2
Number of combinations / 0.04 GeV
Effective mass (GeV)

FIG. 6

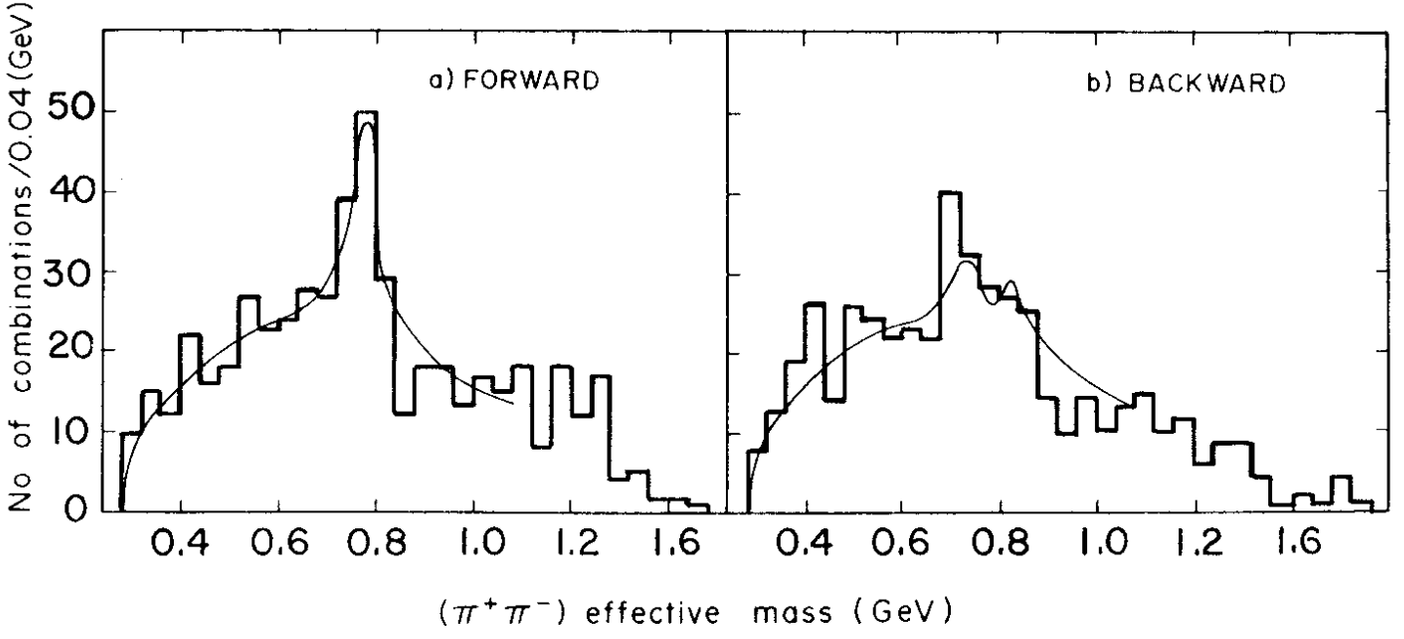
a) FORWARD
b) BACKWARD
No of combinations/0.04 (GeV)
0
10
20
30
40
50
0.4
0.6
0.8
1.0
1.2
1.6
$(\pi^+\pi^-)$ effective mass (GeV)

FIG. 7